Available online at www.sciencedirect.com
ScienceDirect
Journal of Sound and Vibration 324 (2009) 1–25
JOURNAL OF SOUND AND VIBRATION
www.elsevier.com/locate/jsvi

Feedforward control of flexural waves propagating in a rectangular panel

Hiroyuki Iwamoto*, Nobuo Tanaka

Department of Aerospace Engineering, Tokyo Metropolitan University, 6-6 Asahigaoka, Hino-city, Tokyo 191-0065, Japan

Received 1 August 2008; received in revised form 20 January 2009; accepted 6 February 2009
Handling Editor: J. Lam
Available online 10 March 2009

Abstract

This paper is concerned with active wave control of a distributed parameter structure. It is the purpose of this paper to present the active wave control method of a rectangular panel and to clarify fundamental properties of the control system. Firstly, a transfer matrix method for a rectangular panel is introduced to describe the wave dynamics of the structure. This is followed by the derivation of feedforward control laws for absorbing reflected waves or eliminating transmitted waves. In the proposed method, the control laws are including the modal actuation scheme for uncontrolled direction. Then, from a viewpoint of numerical analyses, basic properties of the proposed method are verified. It is found that the reflected wave absorbing control enables the inactivation of all vibration modes in the controlled direction and the transmitted wave eliminating control enables the generation of an almost vibration-free state. It is also found that some phenomena different from the case of a beam-like structure appear under certain boundary conditions.

1. Introduction

According to the recent advances in microprocessors, active control of a flexible structure has become a realizable method for suppressing the vibration. Although many control methods have been proposed regardless of feedforward or feedback control, the mainstream of active vibration control of a flexible structure is modal-based approach which is based on modal analyses [1–5]. However, this method encounters difficulties in controlling a distributed parameter structure such as a flexible beam, a panel structure and so on since such a structure has an infinite number of vibration modes. Furthermore, the conventional modal model cannot be sufficiently accurate over a modally rich frequency range since modal frequencies and eigenfunctions are extremely sensitive to inevitable modelling errors. To overcome this problem, active wave control has been studied in recent years [6–22]. The wave-based approach is based on the hypothesis of modal

*Corresponding author.
E-mail address: hiwamoto@sd.tmu.ac.jp (H. Iwamoto).

0022-460X/$ - see front matter © 2009 Elsevier Ltd. All rights reserved.
doi:10.1016/j.jsv.2009.02.009

excitation mechanism described below;

(1) A disturbance force excites a target structure.
(2) Excitation energy propagates through the structure in the form of travelling waves.
(3) When the travelling waves reach the structural boundary, reflected waves are produced according to the boundary condition.
(4) The interference of travelling and reflected waves results in forming standing waves.
(5) If the shape of the standing wave accords with the mode shape, then the vibration modes are excited.

If the vibration phenomenon is expressed by a fourth-order partial differential equation, near-fields that decay from boundaries appear in the process of modal excitation. However, those components do not have an essential contribution to resonance phenomena.

As written in the above hypothesis, the standing waves are the direct cause of modal excitation. In other words, the vibration modes cannot be excited without the standing waves. Hence, if the reflected waves are eliminated with any control input, then no standing waves are produced, resulting in the inactivation of vibration modes. This is the concept of an active wave control method. Furthermore, active wave control enables to realize an almost vibration-free state in a far-field of the controlled region by eliminating the wave transmitting through the control point from disturbance side to downstream since there are no external inputs except the control forces in the downstream region. Thus, the active wave control method has the two unique control effects as compared to conventional control methods.

Reviewing the literature regarding active wave control, most of the control methods are proposed for a one-dimensional structure such as a flexible beam [6–18]. Those methods were studied from a viewpoint of feedback control [6–10] and feedforward control [11–18]. In the case of feedforward control for a finite structure, wave filtering methods which directly extract the designated wave amplitude [15–18] were presented in order to experimentally construct the control system based on an adaptive technique such as filtered-x LMS algorithm. In contrast to the one-dimensional case, there are few reports on two-dimensional active wave control [19–22]. As an example dealing with a semi-infinite panel, Pan and Hansen [19] presented power transmission control along a semi-infinite panel using in-phase or independent control forces, and investigated the theoretically achievable reduction for each type of control forces. Furthermore, Young and Hansen [20] presented active control of wave transmission using PZT stack actuators placed between a stiffener flange and a semi-infinite panel (although they also attempted to control a finite rectangular panel, it was not active wave control since it aims to suppress error signals at certain points in the controlled region). With the similar concept, Kessissoglou [21,22] analytically and experimentally studied active control of the bending wave transmission through the reinforcing beam of a ribbed and semi-infinite panel. In the case of a finite structure, Sakano and Tanaka [23] proposed active wave control for generating a quite zone in a finite and pinned-supported panel by decomposing eigenfunctions into two wave components; positive travelling wave and negative travelling wave. However, this method is not a natural extension of the one-dimensional active wave control, and hence its control effects are far less than the ideal result which is expected from the one-dimensional case.

This paper presents the active wave control method for a finite rectangular panel in order to naturally extend a one-dimensional case, clarifying the fundamental properties of the control system. Firstly, a transfer matrix method for a rectangular panel is introduced to describe the wave dynamics of the structure. This is followed by the derivation of feedforward control laws for absorbing reflected waves or eliminating transmitted waves. In the proposed method, the control laws are including the modal actuation scheme for uncontrolled direction. Then, from a viewpoint of numerical analyses, control effects of the proposed method are verified. It is found that the reflected wave absorbing control (RWAC) enables the inactivation of all vibration modes in the controlled direction and the transmitted wave eliminating control (TWEC) enables the generation of an almost vibration-free state. It is also found that some phenomena different from the case of a beam-like structure appear under certain boundary conditions.

2. Derivation of transfer matrices of a rectangular panel

In the conventional modelling method for designing a control system, the structural dynamics is expressed in terms of only vibration modes. This paper, however, places an emphasis on the wave motion in the target structure, so that a transfer matrix method is introduced which is based on a wave solution of a rectangular panel. Provided that shear deformation and rotary inertia are negligible, a displacement of a rectangular panel, $w(x,y,t)$, satisfies the following equation:

$$D\nabla^2\nabla^2 w(x,y,t) + \rho h \frac{\partial^2 w(x,y,t)}{\partial t^2} = f(x,y,t), \tag{1}$$

where D is the flexural rigidity, ∇^2 the Laplacian, ρ the mass density per unit volume of the panel, h the panel thickness and a function, $f(x,y,t)$, is an external input applied to the panel, respectively. Assuming that the structure is subjected to the harmonic excitation, the time-dependent term of Eq. (1) is $e^{j\omega t}$. If this is the case, a general solution to Eq. (1) is given by

$$\begin{aligned} w(x,y,t) &= w(x,y)e^{j\omega t} \\ &= \sum_{l=1}^{\infty} W_l(x,y)e^{j\omega t}. \end{aligned} \tag{2}$$

In the conventional modal analysis, $W_l(x,y)$ in the above equation is expressed as the product of a modal coefficient and a normalized modal function. This paper, however, aims to express the structural vibration by wave motion, employing the separation of the spatial function $W_l(x,y)$ for each direction, that is

$$W_l(x,y) = w_m(x)w_n(y), \tag{3}$$

where m and n denote the modal index in the x and y direction, respectively. Note that Eq. (2) is valid if $w_m(x)$ or $w_n(y)$ is a harmonic function. In this paper, the latter is assumed to be a harmonic function. If this is the case, $w_n(y)$ satisfies the following equation:

$$\frac{d^2 w_n(y)}{dy^2} = -\beta_n^2 w_n(y), \tag{4}$$

where β_n is a wavenumber in the y direction. It should be noted that the classical boundary conditions which satisfy this assumption are a pinned support and a sliding support. However, in the region where the near-field effect is relatively small, the assumption in Eq. (4) approximately holds.

Then, substituting Eqs. (2)–(4) into a homogeneous equation of Eq. (1) yields

$$\sum_{m=1,n=1}^{\infty} \left\{ \frac{d^4 w_m(x)}{dx^4} - 2\beta_n^2 \frac{d^2 w_m(x)}{dx^2} + (\beta_n^4 - k^4) w_m(x) \right\} = 0, \tag{5}$$

where

$$k^4 = \frac{\rho h \omega^2}{D}. \tag{6}$$

Solving Eq. (5), the progressive wave solution in the x direction of the panel is derived as

$$w_m(x) = c_1 e^{a_n x} + c_2 e^{b_n x} + c_3 e^{-a_n x} + c_4 e^{-b_n x}, \tag{7}$$

where c_1, c_2, c_3 and c_4 are the coefficients defined by the boundary conditions at $x = 0$ and $x = Lx$. Furthermore, a_n and b_n are described as

$$a_n = \sqrt{\beta_n^2 + k^2}, \tag{8}$$

$$b_n = \sqrt{\beta_n^2 - k^2}. \tag{9}$$

It should be noted that the second and fourth terms in the right-hand side of Eq. (7) become a complex exponential function if b_n becomes an imaginary number. Therefore, there are not always progressive waves in the structural vibration. By using Eqs. (6) and (9), the frequencies at which progressive waves begin to propagate and these reflect from the boundaries parallel to the y-axis are derived as

$$\omega_{c,n} = \sqrt{\frac{D}{\rho h}}\beta_n^2 \tag{10}$$

and these are termed *cut-on frequencies*. As is apparent from the above equation, cut-on frequencies exist for each modal index in the y direction, n.

Next, substituting Eqs. (3) and (7) into Eq. (2), a solution to Eq. (1) is written as

$$w(x,y) = \sum_{n=1}^{\infty}(c_{1,n}\mathrm{e}^{a_n x} + c_{2,n}\mathrm{e}^{b_n x} + c_{3,n}\mathrm{e}^{-a_n x} + c_{4,n}\mathrm{e}^{-b_n x})w_n(y). \tag{11}$$

Applying the formulae provided by material mechanics to Eq. (11), slope $\theta_x(x,y)$, internal bending moment $m_x(x,y)$ and internal shear force $q_x(x,y)$ in the x direction are obtained. The state vector $\mathbf{z}(x,y)$ at arbitrary position on the rectangular panel is then defined as

$$\mathbf{z}(x,y) = [w(x,y) \quad \theta_x(x,y) \quad m_x(x,y) \quad q_x(x,y)]^{\mathrm{T}} = \sum_{n=1}^{\infty}\mathbf{z}_n(x)w_n(y), \tag{12}$$

where the superscript T denotes the transpose of the expression, and $\mathbf{z}_n(x)$ is the state vector in the x direction at modal index, n, which is defined as

$$\mathbf{z}_n(x) = [w_n(x) \;\; \theta_{x,n}(x) \;\; m_{x,n}(x)/D \;\; q_{x,n}(x)/D]^{\mathrm{T}} = \mathbf{K}_n\mathbf{D}_n(x)\mathbf{c}_n, \tag{13}$$

where

$$\mathbf{K}_n = \begin{bmatrix} 1 & 1 & 1 & 1 \\ -a_n & -b_n & a_n & b_n \\ \nu\beta_n^2 - a_n & \nu\beta_n^2 - a_n & \nu\beta_n^2 - b_n & \nu\beta_n^2 - b_n \\ a_n(\beta_n^2 - a_n^2) & b_n(\beta_n^2 - b_n^2) & -a_n(\beta_n^2 - a_n^2) & -b_n(\beta_n^2 - b_n^2) \end{bmatrix}, \tag{14}$$

$$\mathbf{D}_n(x) = \begin{bmatrix} \mathrm{e}^{a_n x} & 0 & 0 & 0 \\ 0 & \mathrm{e}^{b_n x} & 0 & 0 \\ 0 & 0 & \mathrm{e}^{-a_n x} & 0 \\ 0 & 0 & 0 & \mathrm{e}^{-b_n x} \end{bmatrix}, \tag{15}$$

$$\mathbf{c}_n = [c_{1,n} \;\; c_{2,n} \;\; c_{3,n} \;\; c_{4,n}]^{\mathrm{T}}. \tag{16}$$

Next, consider a panel element along the x-axis with node $i-1$ and i at both ends of the element as shown in Fig. 1. Let $\mathbf{z}_n(x_{i-1})$ and $\mathbf{z}_n(x_i)$ be ${}_{i-1}\mathbf{z}_n$ and ${}_i\mathbf{z}_n$ for brevity, and apply a local coordinate to these state vectors. Hence, by setting ${}_{i-1}\mathbf{z}_n$ to be a local origin, ${}_i\mathbf{z}_n$ is written as a function of the distance between the two nodes, l. Then, from Eqs. (13) and (15), the state vectors at each node are described as

$${}_{i-1}\mathbf{z}_n = \mathbf{K}_n\mathbf{D}_n(0)\mathbf{c}_n = \mathbf{K}_n\mathbf{c}_n, \tag{17}$$

$${}_i\mathbf{z}_n = \mathbf{K}_n\mathbf{D}_n(l)\mathbf{c}_n. \tag{18}$$

Multiplying Eq. (17) by $\mathbf{K}_n^{-1}$ and substituting the resultant equation into Eq. (18) leads to the state equation of a panel expressed in the form

$${}_i\mathbf{z}_n = \mathbf{K}_n\mathbf{D}_n(l)\mathbf{K}_n^{-1}{}_{i-1}\mathbf{z}_n = {}_{i,i-1}\mathbf{T}_n{}_{i-1}\mathbf{z}_n, \tag{19}$$

where ${}_{i,i-1}\mathbf{T}_n$ denotes the transfer matrix of the state vectors in the x direction at modal index, n, between the node $i-1$ and i. Next, applying the coordinate transformation to $\mathbf{z}_n$ by the matrix $\mathbf{K}_n$, the wave vector, $\mathbf{w}_n(x)$,

may be defined as

$$\mathbf{w}_n(x) = [c_{1,n}e^{a_n x} \;\; c_{2,n}e^{b_n x} \;\; c_{3,n}e^{-a_n x} \;\; c_{4,n}e^{-b_n x}]^{\mathrm{T}} = \mathbf{K}_n^{-1}\mathbf{z}_n(x). \tag{20}$$

Furthermore, substituting Eq. (20) into Eq. (19) leads to

$${}_i\mathbf{w}_n = \mathbf{D}_n(l)_{i-1}\mathbf{w}_n. \tag{21}$$

As seen from Eq. (21), the matrix $\mathbf{D}_n$ is found to be a transfer matrix of the wave vectors.

Next, consider the case where a disturbance force f_d acts at node 2 and Nc control forces ($f_1, f_2, \ldots, f_{Nc}$) placed parallel to the y-axis act to node 1 as shown in Fig. 2(a). The state equation of the rectangular panel in the

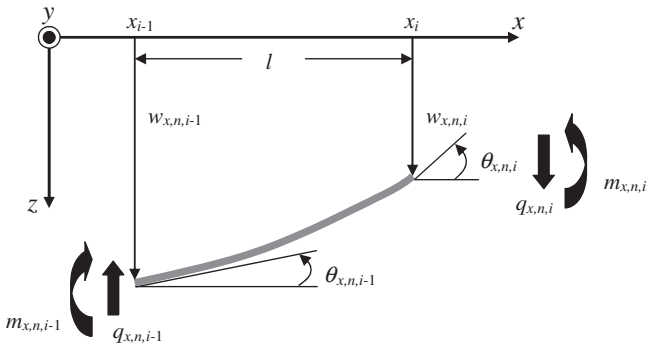

Fig. 1. Cross section of a panel element parallel to the x-axis.

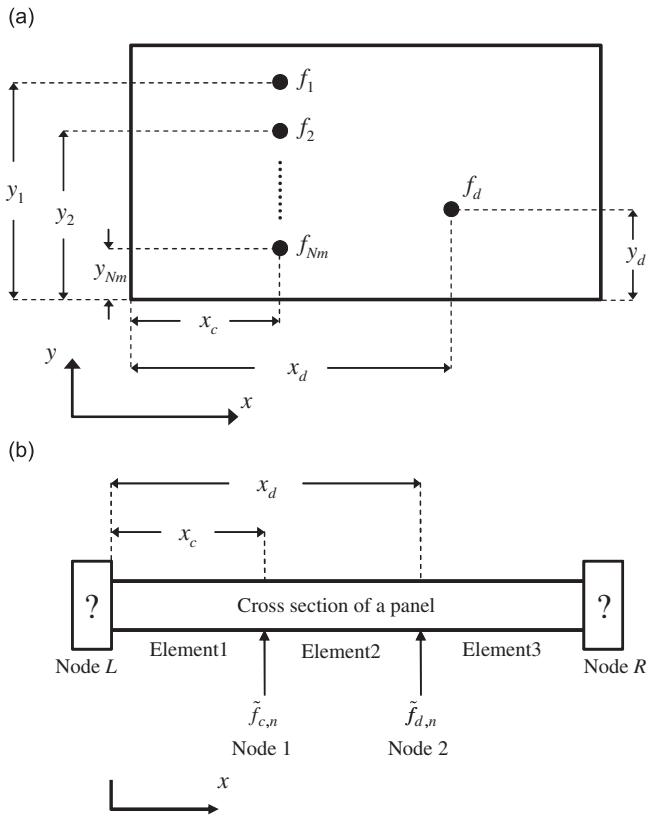

Fig. 2. Rectangular panel with control and disturbance forces. (a) Physical coordinate system. (b) Coordinate system in a transfer matrix method.

Table 1
Relation between four classical boundary conditions and the indices in the state vector at $x = 0$ and $x = L_x$.

	$x = 0$	$x = L_x$
Pinned support ($w = 0$, $m_x = 0$)	$p = 2$, $q = 4$	$i = 1$, $j = 3$
Free end ($m_x = 0$, $q_x = 0$)	$p = 1$, $q = 2$	$i = 3$, $j = 4$
Clamped support ($w = 0$, $\theta = 0$)	$p = 3$, $q = 4$	$i = 1$, $j = 2$
Sliding support ($w = 0$, $q_x = 0$)	$p = 1$, $q = 3$	$i = 2$, $j = 4$

x direction at modal index, n, is then written as

$$ {}_R\mathbf{z}_n = {}_{R,L}\mathbf{T}_n {}_L\mathbf{z}_n + {}_{R,1}\mathbf{T}_n\mathbf{f}_{c,n} + {}_{R,2}\mathbf{T}_n\mathbf{f}_{d,n}, \tag{22} $$

where

$$ \mathbf{f}_{c,n} = [0\ \ 0\ \ 0\ \ 0\ \ \tilde{f}_{c,n}/D]^{\mathrm{T}}, \quad \tilde{f}_{c,n} = c_f \sum_{l=1}^{Nc} f_l w_n(y_l), \tag{23} $$

$$ \mathbf{f}_{d,n} = [0\ \ 0\ \ 0\ \ 0\ \ \tilde{f}_{d,n}/D]^{\mathrm{T}}, \quad \tilde{f}_{d,n} = c_f f_d w_n(y_d), \tag{24} $$

where c_f is a constant determined by the boundary conditions at $y = 0$ and $y = L_y$. Here, the boundary conditions at $x = 0$ and $x = L_x$ are given by setting two out of four state variables in the state vector to be zero. Supposing that the ith and jth state variables at the right end are zero, and the pth and qth state variables at the left end, ${}_L\mathbf{z}_{p,n}$ and ${}_L\mathbf{z}_{q,n}$, are non-zero, Eq. (22) expands to the following equations:

$$ {}_{R,L}t_{ip,n}\,{}_Lz_{p,n} + {}_{R,L}t_{iq,n}\,{}_Lz_{q,n} + {}_{R,1}t_{i4,n}\tilde{f}_{c,n} + {}_{R,2}t_{i4,n}\tilde{f}_{d,n} = 0, \tag{25} $$

$$ {}_{R,L}t_{jp,n}\,{}_Lz_{p,n} + {}_{R,L}t_{jq,n}\,{}_Lz_{q,n} + {}_{R,1}t_{j4,n}\tilde{f}_{c,n} + {}_{R,2}t_{j4,n}\tilde{f}_{d,n} = 0, \tag{26} $$

where ${}_{ij}t_{kl}$ denotes the kth row and lth column variable in the transfer matrix $\mathbf{T}_{ij}$. Then, from Eqs. (25) and (26), the non-zero state variables at the left end (node L) are given by

$$ {}_Lz_{p,n} = -(\alpha_{11,n}\tilde{f}_{c,n} + \alpha_{12,n}\tilde{f}_{d,n})/D\Delta_n, \tag{27} $$

$$ {}_Lz_{q,n} = -(\alpha_{21,n}\tilde{f}_{c,n} + \alpha_{22,n}\tilde{f}_{d,n})/D\Delta_n, \tag{28} $$

where

$$ \alpha_{11,n} = {}_{R,L}t_{jq,n}\,{}_{R,1}t_{i4,n} - {}_{R,L}t_{iq,n}\,{}_{R,1}t_{j4,n}, \tag{29} $$

$$ \alpha_{12,n} = {}_{R,L}t_{jq,n}\,{}_{R,2}t_{i4,n} - {}_{R,L}t_{iq,n}\,{}_{R,2}t_{j4,n}, \tag{30} $$

$$ \alpha_{21,n} = {}_{R,L}t_{ip,n}\,{}_{R,1}t_{j4,n} - {}_{R,L}t_{jp,n}\,{}_{R,1}t_{i4,n}, \tag{31} $$

$$ \alpha_{22,n} = {}_{R,L}t_{ip,n}\,{}_{R,2}t_{j4,n} - {}_{R,L}t_{jp,n}\,{}_{R,2}t_{i4,n}, \tag{32} $$

$$ \Delta_n = {}_{R,L}t_{ip,n}\,{}_{R,L}t_{jq,n} - {}_{R,L}t_{iq,n}\,{}_{R,L}t_{jp,n}. \tag{33} $$

Thus, boundary conditions are given by setting i, j, p and q. The relations between those indices and four classical boundary conditions are listed in Table 1.

3. Derivation of the active control laws for a rectangular panel

In this section, two control laws are derived; one is the RWAC and the other is the TWEC as mentioned in Section 1. As will be shown in the next section, each control law enables the unique control effect.

First of all, the control law of the RWAC is derived. In this case, a reflected wave is defined as the wave propagating from a control point (node 1) to a disturbance point (node 2), that is, a positive travelling wave in

Element 2 as shown in Fig. 2(b). The wave vector at arbitrary position (node a) in Element 2 is given by

$$ {}_a\mathbf{w}_n = \mathbf{K}_n^{-1}{}_a\mathbf{z}_n = \mathbf{K}_n^{-1}{}_{a,1}\mathbf{T}_n({}_{1,L}\mathbf{T}_{nL}\mathbf{z}_n + \mathbf{f}_{c,n}), \tag{34} $$

where

$$ \mathbf{K}_n^{-1}{}_{a,1}\mathbf{T}_n = \frac{1}{2(a_n^2 - b_n^2)} \begin{bmatrix} \mathrm{e}^{a_n x}(\nu\beta_n^2 - b_n^2) & -\mathrm{e}^{a_n x}(\beta_n^2 - b_n^2)/a_n & -\mathrm{e}^{a_n x} & -\mathrm{e}^{a_n x}/a_n \\ \mathrm{e}^{b_n x}(a_n^2 - \nu\beta_n^2) & -\mathrm{e}^{b_n x}(a_n^2 - \beta_n^2)/b_n & \mathrm{e}^{b_n x} & \mathrm{e}^{b_n x}/b_n \\ \mathrm{e}^{-a_n x}(\nu\beta_n^2 - b_n^2) & \mathrm{e}^{-a_n x}(\beta_n^2 - b_n^2)/a_n & -\mathrm{e}^{-a_n x} & \mathrm{e}^{-a_n x}/a_n \\ \mathrm{e}^{-b_n x}(a_n^2 - \nu\beta_n^2) & \mathrm{e}^{-b_n x}(a_n^2 - \beta_n^2)/a_n & \mathrm{e}^{-b_n x} & -\mathrm{e}^{-b_n x}/b_n \end{bmatrix}. \tag{35} $$

Furthermore, the term remaining in Eq. (34) is given by

$$ {}_{1,L}\mathbf{T}_{nL}\mathbf{z}_n + \mathbf{f}_{c,n} = \begin{bmatrix} \varepsilon_{1,n}\tilde{f}_{c,n} + \varepsilon_{2,n}\tilde{f}_{d,n} \\ \varepsilon_{3,n}\tilde{f}_{c,n} + \varepsilon_{4,n}\tilde{f}_{d,n} \\ \varepsilon_{5,n}\tilde{f}_{c,n} + \varepsilon_{6,n}\tilde{f}_{d,n} \\ \varepsilon_{7,n}\tilde{f}_{c,n} + \varepsilon_{8,n}\tilde{f}_{d,n} \end{bmatrix}, \tag{36} $$

where

$$ \varepsilon_{1,n} = -({}_{1,L}t_{1p,n}\alpha_{11,n} + {}_{1,L}t_{1q,n}\alpha_{21,n})/D\Delta_n, \tag{37} $$

$$ \varepsilon_{2,n} = -({}_{1,L}t_{1p,n}\alpha_{12,n} + {}_{1,L}t_{1q,n}\alpha_{22,n})/D\Delta_n, \tag{38} $$

$$ \varepsilon_{3,n} = -({}_{1,L}t_{2p,n}\alpha_{11,n} + {}_{1,L}t_{2q,n}\alpha_{21,n})/D\Delta_n, \tag{39} $$

$$ \varepsilon_{4,n} = -({}_{1,L}t_{2p,n}\alpha_{12,n} + {}_{1,L}t_{2q,n}\alpha_{22,n})/D\Delta_n, \tag{40} $$

$$ \varepsilon_{5,n} = -({}_{1,L}t_{3p,n}\alpha_{11,n} + {}_{1,L}t_{3q,n}\alpha_{21,n})/D\Delta_n, \tag{41} $$

$$ \varepsilon_{6,n} = -({}_{1,L}t_{3p,n}\alpha_{12,n} + {}_{1,L}t_{3q,n}\alpha_{22,n})/D\Delta_n, \tag{42} $$

$$ \varepsilon_{7,n} = -({}_{1,L}t_{4p,n}\alpha_{11,n} + {}_{1,L}t_{4q,n}\alpha_{21,n} - \Delta_n)/D\Delta_n, \tag{43} $$

$$ \varepsilon_{8,n} = -({}_{1,L}t_{4p,n}\alpha_{12,n} + {}_{1,L}t_{4q,n}\alpha_{22,n})/D\Delta_n. \tag{44} $$

Substituting Eqs. (35)–(44) into Eq. (34), and nullifying the target wave component, the feedforward control force of the RWAC in the coordinate system shown in Fig. 2(b) is derived as

$$ \tilde{f}_{c,n} = -\tilde{g}_{r,n}\tilde{f}_{d,n}, \tag{45} $$

where $\tilde{g}_{r,n}$ is the control law of the RWAC given by

$$ \tilde{g}_{r,n} = \frac{\varepsilon_{2,n}b_n(a_n^2 - \nu\beta_n^2) + \varepsilon_{4,n}(a_n^2 - \beta_n^2) + \varepsilon_{6,n}b_n - \varepsilon_{8,n}}{\varepsilon_{1,n}b_n(a_n^2 - \nu\beta_n^2) + \varepsilon_{3,n}(a_n^2 - \beta_n^2) + \varepsilon_{5,n}b_n - \varepsilon_{7,n}}. \tag{46} $$

It should be noted that the control force described in Eq. (45) is for the vibration component with modal index, n. Provided that the target modal index is from 1 to Nm, substituting Eqs. (23) and (24) into Eq. (45)

yields the relation between the control forces and a disturbance force in the matrix form as follows;

$$\begin{bmatrix} w_1(y_1) & w_1(y_2) & \cdots & w_1(y_{Nc}) \\ w_2(y_1) & w_2(y_2) & \cdots & w_2(y_{Nc}) \\ \vdots & \vdots & \ddots & \vdots \\ w_{Nm}(y_1) & w_{Nm}(y_2) & \cdots & w_{Nm}(y_{Nc}) \end{bmatrix} \begin{bmatrix} f_1 \\ f_2 \\ \vdots \\ f_{Nc} \end{bmatrix} = - \begin{bmatrix} w_1(y_d)\tilde{g}_{r,1} \\ w_2(y_d)\tilde{g}_{r,2} \\ \vdots \\ w_{Nm}(y_d)\tilde{g}_{r,Nm} \end{bmatrix} f_d$$

$$\mathbf{W}_{yc}\mathbf{f}_c = -\mathbf{g}_r f_d. \tag{47}$$

Therefore, using the Moore–Penrose generalized inverse matrix, the control forces in the physical coordinate system are derived as

$$\mathbf{f}_c = -(\mathbf{W}_{yc}^{\mathrm{T}}\mathbf{W}_{yc})^{-1}\mathbf{W}_{yc}^{\mathrm{T}}\mathbf{g}_r f_d. \tag{48}$$

It is found from the above equation that the control laws include the modal actuation scheme in the y direction [3]. This is because the property of wave propagation depends on the modal index, n, as described in Eqs. (8) and (9), and thus the number of control laws agrees with Nm.

Next, the control law of the TWEC is derived. In this case, a transmitted wave is defined as the wave propagating from a control point to the left end (node L), that is, a negative travelling wave in Element 1 as shown in Fig. 2(b). The wave vector at arbitrary position (node a) in Element 1 is given by

$${}_a\mathbf{w}_n = \mathbf{K}_n^{-1}{}_a\mathbf{z}_n = \mathbf{K}_n^{-1}{}_{a,1}\mathbf{T}_{nL}\mathbf{z}_n. \tag{49}$$

Substituting Eqs. (14) and (15) into Eq. (49), and nullifying the target wave component, the feedforward control force of TWEC in the coordinate system shown in Fig. 2(b) is derived as

$$\tilde{f}_{c,n} = -\tilde{g}_{t,n}\tilde{f}_{d,n}, \tag{50}$$

where $\tilde{g}_{t,n}$ is the control law of TWEC given by

$$\tilde{g}_{t,n} = \frac{\kappa_{p,n}\alpha_{12,n} + \kappa_{q,n}\alpha_{22,n}}{\kappa_{p,n}\alpha_{11,n} + \kappa_{q,n}\alpha_{21,n}}, \tag{51}$$

where

$$\kappa_{1,n} = b_n(a_n^2 - \nu\beta_n^2), \quad \kappa_{2,n} = -(a_n^2 - \beta_n^2), \quad \kappa_{3,n} = b_n, \quad \kappa_{4,n} = 1. \tag{52}$$

Then, taking the same procedure as the case of the RWAC, the control forces in the physical coordinate are derived as

$$\mathbf{f}_c = -(\mathbf{W}_{yc}^{\mathrm{T}}\mathbf{W}_{yc})^{-1}\mathbf{W}_{yc}^{\mathrm{T}}\mathbf{g}_t f_d, \tag{53}$$

where

$$\mathbf{g}_t = [w_1(y_d)\tilde{g}_{t,1} \;\; w_2(y_d)\tilde{g}_{r,2} \;\; \cdots \;\; w_{Nm}(y_d)\tilde{g}_{r,Nm}]^{\mathrm{T}}. \tag{54}$$

As with other active wave control strategies, the control laws given by Eqs. (46) and (51) are non-causal, so that it is necessary to approximately realize the ideal filters when the control system is constructed. One of the resolution methods is to approximate it with causal filter in a band-limited spectrum [7,15–18], which makes it possible to obtain the almost ideal control effects.

4. Numerical simulation

This section presents the control effects of the proposed method from a viewpoint of frequency response and displacement distribution using physical and geometric properties of the panel listed in Table 2(a). For the evaluation of displacement distribution, absolute envelope and time histories along the lines at $x = 1.13$ m and $y = 0.11$ m are used. The time history plots are necessary to show a wave propagation state at the exciting frequency. Although the displacement distributions are evaluated at certain resonance frequencies as

examples, the same control effects are obtained at other resonance frequencies in each case. Unlike the analytical development discussed in the previous sections, the numerical analysis deals with a small amount of loss factor, $\eta = 0.003$, which is necessary to avoid numerical overflow at modal frequencies of the panel. The minute loss factor, however, will not have any significant influence on the simulation reliability. Furthermore, as previously described, $w_n(y)$ must be a harmonic function, so that it is assumed that the boundary condition at $y = 0$ and $y = L_y$ is the pinned support in the simulation. If this is the case, the following equations are determined:

$$w_n(y) = \sin \beta_n x, \quad \beta_n = \frac{n\pi}{L_y}, \quad c_f = \frac{2}{L_y}. \tag{55}$$

The disturbance point is fixed at $(x_d, y_d) = (1.13\,\text{m}, 0.11\,\text{m})$ through the simulation, and the target modal index is up to 3. Moreover, the four control forces are placed parallel to the y-axis that are located in the y direction at $y_1 = 0.21\,\text{m}$, $y_2 = 0.32\,\text{m}$, $y_3 = 0.43\,\text{m}$, and $y_4 = 0.54\,\text{m}$, respectively.

In the case of active wave control for a beam-like structure, its control effects are the same for any boundary condition [13]. However, as will be shown later, the control effects of active wave control for a finite rectangular panel are dominated by the boundary conditions.

Table 2
Physical parameters of the rectangular panel and the corresponding cut-on frequencies.

(a) Physical parameters

Length in the x direction (m)	Length in the y direction (m)	Thickness (m)	Young's modulus (N/m^2)	Density (kg/m^3)	Poisson's ratio
1.2	0.63	4×10^{-3}	2.06×10^{11}	7900	0.29

(b) Cut-on frequencies (Hz)

First	Second	Third
24.38	97.54	219.46

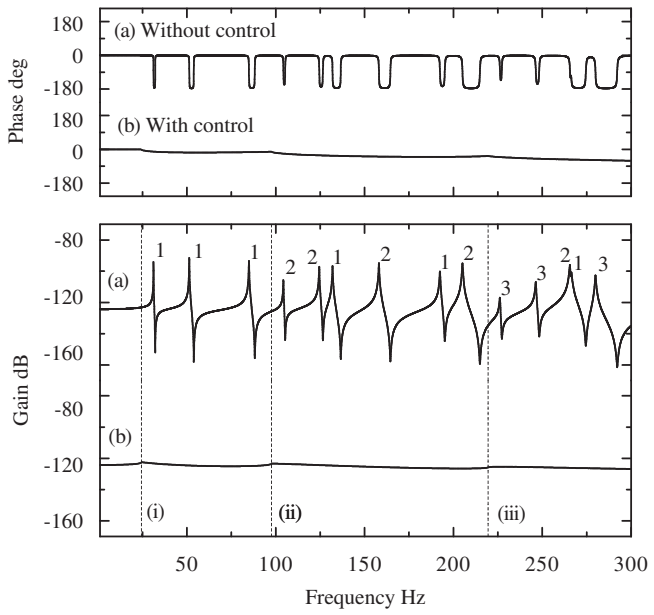

Fig. 3. Driving point compliances of the panel with and without the RWAC when the boundary conditions at the both ends of the panel are the pinned support; the vertical dash lines indicate the first three cut-on frequencies.

4.1. Control effects of the RWAC

In this paper, three cases of the boundary conditions at $x = 0$ and $x = L_x$ are considered to clarify the properties of the RWAC, that is, (i) the pinned support ($\xi = 0, m = 0$), (ii) the free end ($m = 0, q = 0$), and (iii) the sliding support ($\theta = 0, q = 0$). The position of the control forces array in the x direction is fixed at $x_c = 0.07$ m. For the evaluation of displacement distribution, the magnitude of the disturbance force and the exciting frequency are different for each case, and these are written in the figures of displacement distribution.

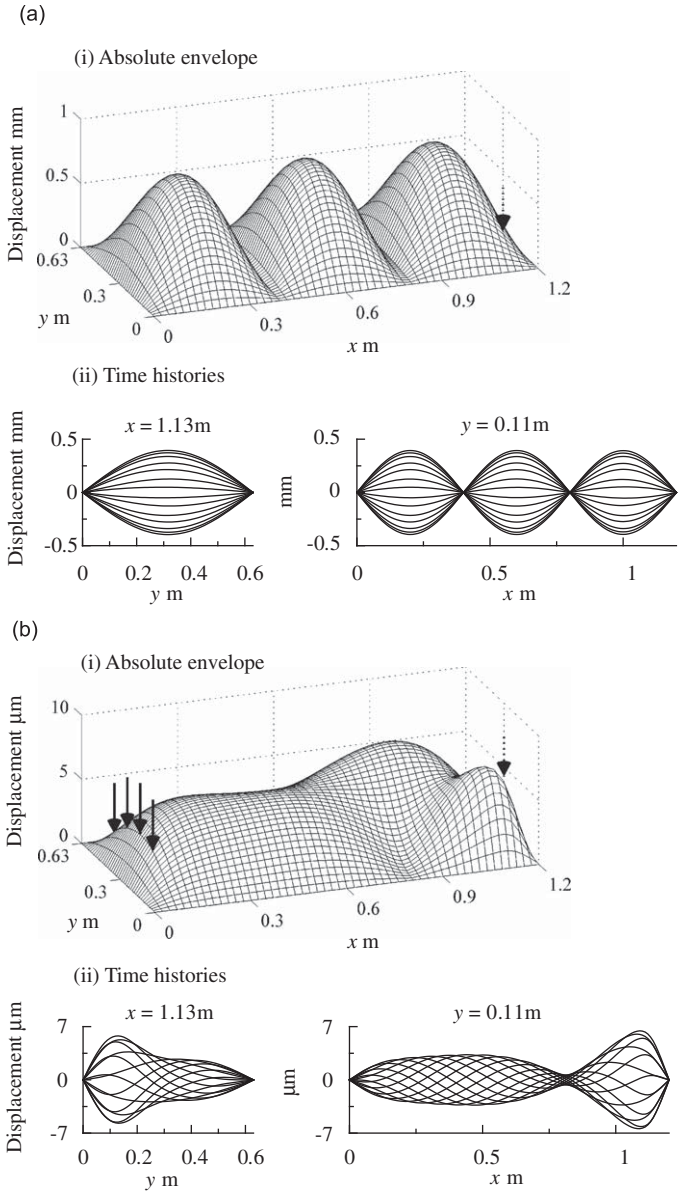

Fig. 4. Envelopes of absolute displacement of the panel at the third modal frequency with and without the RWAC and the corresponding time histories along the lines at $x = 1.13$ m and $y = 0.11$ m when the boundary conditions at the both ends of the panel are the pinned supports; the dotted arrow is a disturbance force and the solid arrows are control forces. (a) Without control (frequency: 84.86 Hz, $f_d = 10$ N): (i) absolute envelope; (ii) time histories. (b) With control (frequency: 84.86 Hz, $f_d = 10$ N): (i) absolute envelope; (ii) time histories.

Furthermore, the driving point compliance is used for evaluating frequency response to check if the same result as the one-dimensional case is obtained.

Case 1: *Pinned support*. In this part, the case is considered where the boundaries at $x = 0$ and $x = L_x$ are pinned-supported. Fig. 3 depicts the driving point compliances of the panel with and without the RWAC. In the case of non-control, there are fourteen vibration modes in the frequency range up to 300 Hz (note that the 12th and 13th modes are close to degeneration around 266 Hz). In this figure, the numbers labelled at each peak indicate the corresponding modal index, n, and the three vertical dashed lines indicate the cut-on frequencies listed in Table 2(b). In contrast, when the RWAC is applied to the panel, all peaks and notches in the gain plot disappear, and the gain curve almost converges along the asymptote. Although this result is similar to the case of the active wave control for a one-dimensional structure, there exists a slight difference; three humps (not peaks) appear in the controlled gain plot and those frequencies are approximately consistent with the cut-on frequencies. This is because the target wave component $c_4 e^{-b_n x}$ changes its property from a near-field to a progressive wave when the exciting frequency becomes higher than the corresponding cut-on frequency. Thus, the humps indicate the transition from near-field suppression to progressive wave cancellation. However, since all modal frequencies are higher than their cut-on frequencies in this case, the control forces inactivate all vibration modes by eliminating the reflected waves.

Next, the control effect is evaluated from a viewpoint of displacement distribution. Fig. 4 illustrates the envelopes of absolute displacement of the panel at the third modal frequency with and without the RWAC and the corresponding time histories. In the case of non-control, the vibration mode is excited since the standing wave coincides with the mode shape. Naturally, the nodal lines appear in the displacement distribution and the maximum amplitude is 0.76 mm. In contrast, when the RWAC is applied to the panel, the nodal lines disappear and progressive waves become dominant in the structural vibration as shown in the time histories. This phenomenon indicates that the standing wave which is the direct cause of modal excitation is suppressed by the RWAC, resulting in the inactivation of vibration modes. The maximum amplitude is reduced to 6.93 μm, which is 0.91 percent of the uncontrolled amplitude.

Case 2: *Free end*. In this part, the case is considered where the boundary conditions at $x = 0$ and $x = L_x$ are free. Fig. 5 shows the driving point compliances of the panel with and without the RWAC. As shown in the figure, in the case of non-control, the frequencies of the lowest order modes at each modal index, n, are lower than the corresponding cut-on frequencies. This is because resonance phenomena are caused by standing

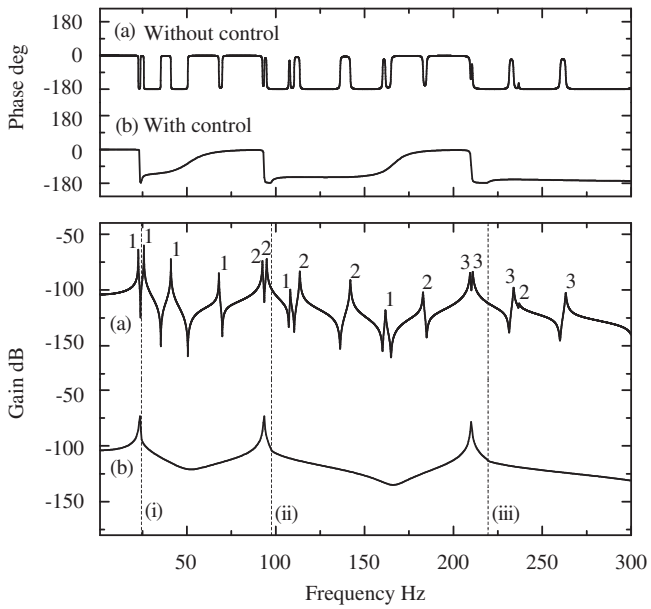

Fig. 5. Driving point compliances of the panel with and without the RWAC when the boundary condition at the both ends of the panel are free; the vertical dash lines indicate the first three cut-on frequencies.

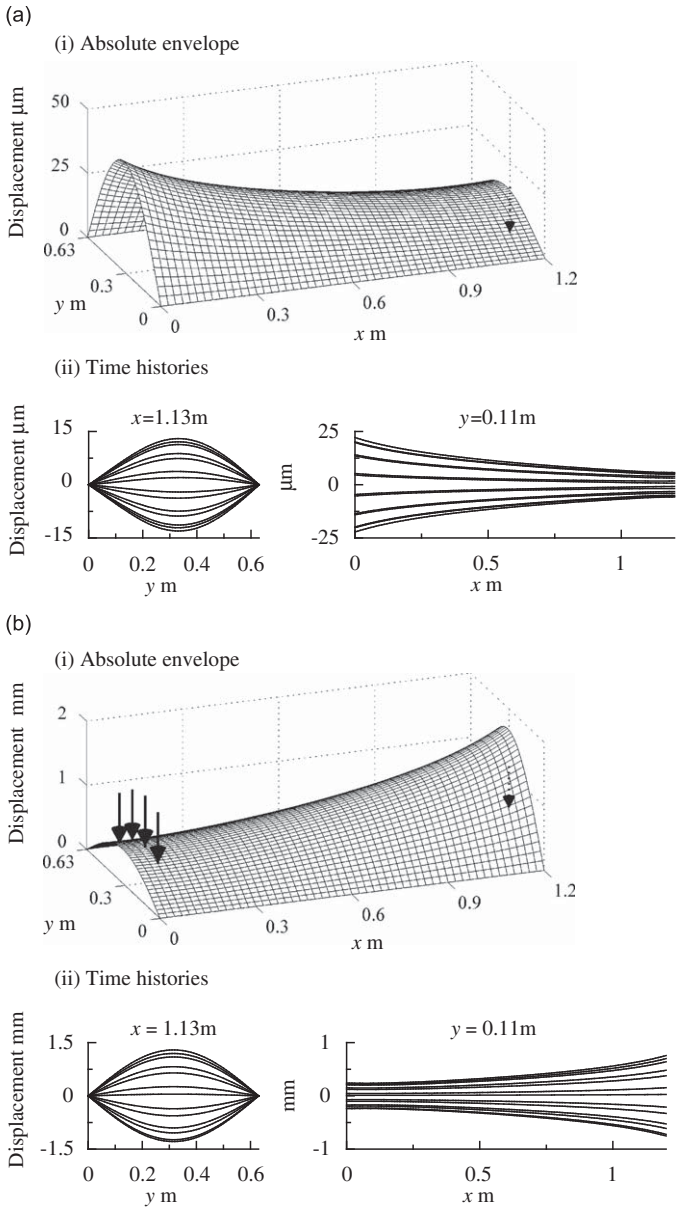

Fig. 6. Envelopes of absolute displacement of the panel at 23.34 Hz with and without the RWAC and the corresponding time histories along the lines at $x = 1.13$ m and $y = 0.11$ m when the boundary conditions at the both ends of the panel are free; the dotted arrow is a disturbance force and the solid arrows are control forces. (a) Without control (frequency: 23.34 Hz, $f_d = 0.5$ N): (i) absolute envelope; (ii) time histories. (b) With control (frequency: 23.34 Hz, $f_d = 0.5$ N): (i) absolute envelope; (ii) time histories.

waves in the y direction. Hence, progressive waves do not exist in the x direction at these modal frequencies, and the near-field components are dominant in this case. After the RWAC is applied to the panel, new vibration modes appear unlike in Case 1. The frequencies of the newly produced modes coincide with those of the pinned-supported beam which has the same length in the y direction and physical parameters as the panel. It means that if the boundary condition of the panel at $x = L_x$ is free, the structure behaves as a one-dimensional structure in the y direction around $x = L_x$ after the reflected waves in the x direction are absorbed by the control inputs. If this is the case, the controlled structure has one vibration mode for each modal index, n, and hence the number of resonance peaks is reduced compared to the case of non-control.

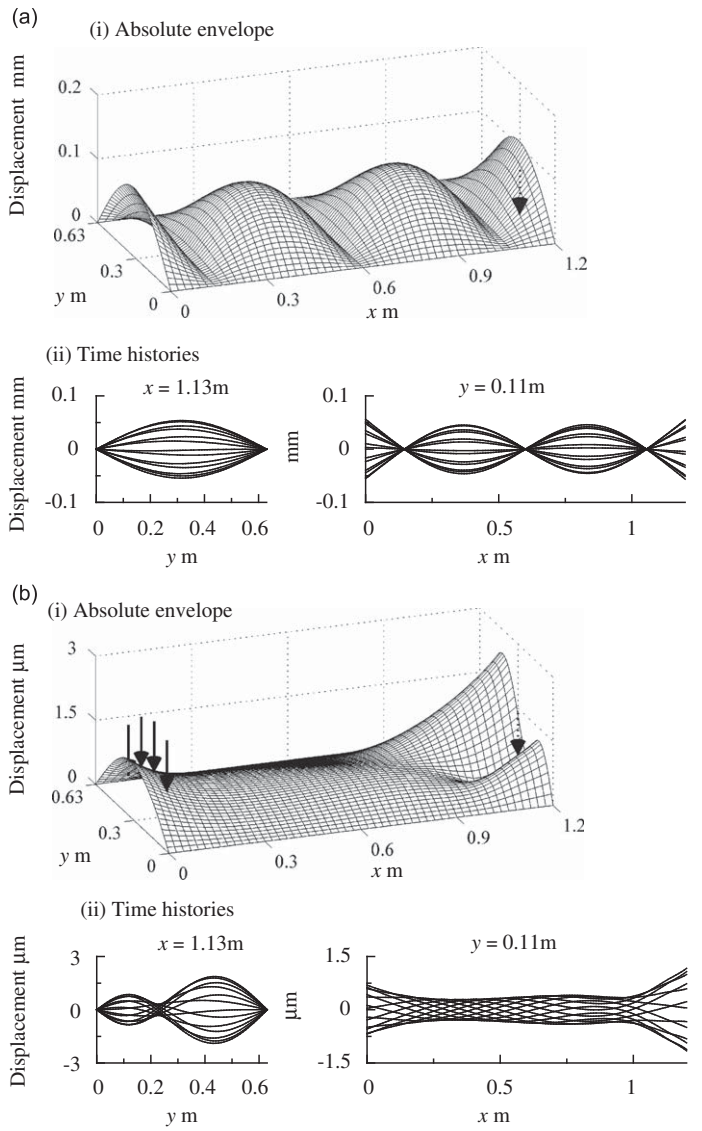

Fig. 7. Envelopes of absolute displacement of the panel at the fourth modal frequency with and without the RWAC and the corresponding time histories along the lines at $x = 1.13$ m and $y = 0.11$ m when the boundary conditions at the both ends of the panel are free; the dotted arrow is a disturbance force and the solid arrows are control forces. (a) Without control (frequency: 67.95 Hz, $f_d = 0.5$ N): (i) absolute envelope; (ii) time histories. (b) With control (frequency: 67.95 Hz, $f_d = 0.5$ N): (i) absolute envelope; (ii) time histories.

Next, consider the displacement distribution at 23.34 Hz where the new vibration mode is produced as shown in Fig. 5. Illustrated in Fig. 6 are the envelopes of absolute displacement of the panel at 23.34 Hz with and without the RWAC and the corresponding time histories. As is apparent from the figure, when the RWAC is applied, the displacement around the line at $x = L_x$ is larger than that in other regions. In this case, the maximum amplitude is 1.46 mm while that of non-control is 42.8 μm. This result implies that after reflected waves in the x direction are absorbed, the structural vibration is strongly dependent on the free end at $x = L_x$, and the panel behaves as one-dimensional structure as mentioned above. Fig. 7 shows the envelopes of absolute displacement of the panel at the fourth modal frequency with and without the RWAC and the corresponding time histories. As with the Case 1, the RWAC reduces the maximum amplitude of the structural vibration from 0.11 mm to 2.44 μm since the vibration mode is made inactive by canceling a reflected wave.

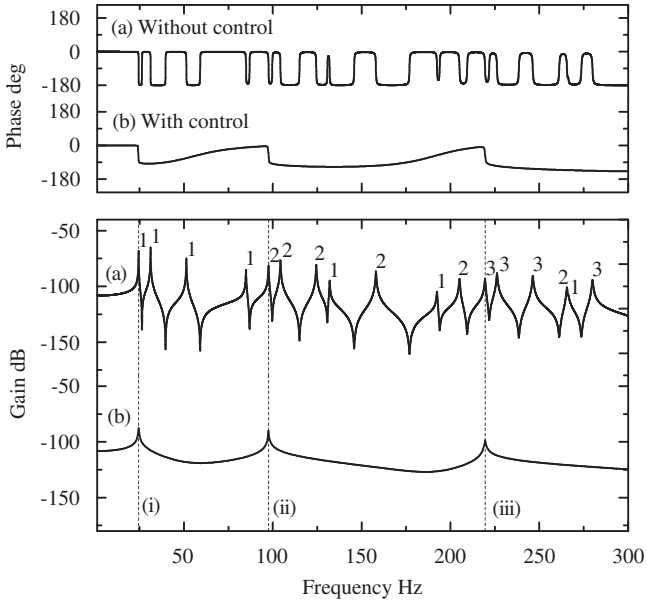

Fig. 8. Driving point compliances of the panel with and without the RWAC when the boundary conditions at the both ends of the panel are the sliding supports.

Case 3: *Sliding support*. In this part, the case is considered where the boundary conditions at $x = 0$ and $x = L_x$ are sliding supports. Fig. 8 illustrates the driving point compliances of the panel with and without the RWAC. It should be noted that the frequencies of the lowest order modes at each modal index, n, coincide with the corresponding cut-on frequencies. At cut-on frequencies, exponential functions of the second and fourth term in the right-hand side of Eq. (7) become constants along the x direction. When the RWAC is applied to the panel, all vibration modes except the lowest order one at each modal index are significantly suppressed, and the frequencies of the residual peaks coincides with those of non-control. As described in the hypothesis of modal excitation, progressive waves that form the standing wave are necessary for the modal excitation. However, the controlled component is a constant in the x direction in this case, so that this term does not much contribute to a resonance phenomenon. Thus, the peaks of the lowest order modes at each modal index remain after control.

Depicted in Fig. 9 are the envelopes of absolute displacement of the panel at the first modal frequency with and without the RWAC and the corresponding time histories. It should be noted that when no control is applied to the panel, the displacement distribution in the x direction is constant. Therefore, the second and fourth terms in Eq. (7) are dominant in the displacement since those are constant at this frequency as previously mentioned. In contrast, if the RWAC is applied, near-field components slightly appear in the vibration in the x direction. In this case, the maximum amplitude is reduced from 0.46 mm to 85.6 μm. However, this reduction is relatively low compared to the case where a vibration mode is made inactive at a modal frequency. Fig. 10 illustrates the envelopes of absolute displacement of the panel at the sixth modal frequency with and without the RWAC and the corresponding time histories. In contrast to the above case, it is found from the figure that the vibration mode is made inactive by the RWAC since the exciting frequency is higher than the corresponding cut-on frequency, and the maximum amplitude is 2.43 μm which is 2.86 percent of non-control.

4.2. Control effects of the TWEC

In this section, the control effects of the TWEC are evaluated. Three cases of the boundary condition at $x = 0$ and $x = L_x$ that are the same as the case of the RWAC are considered. The magnitude of the

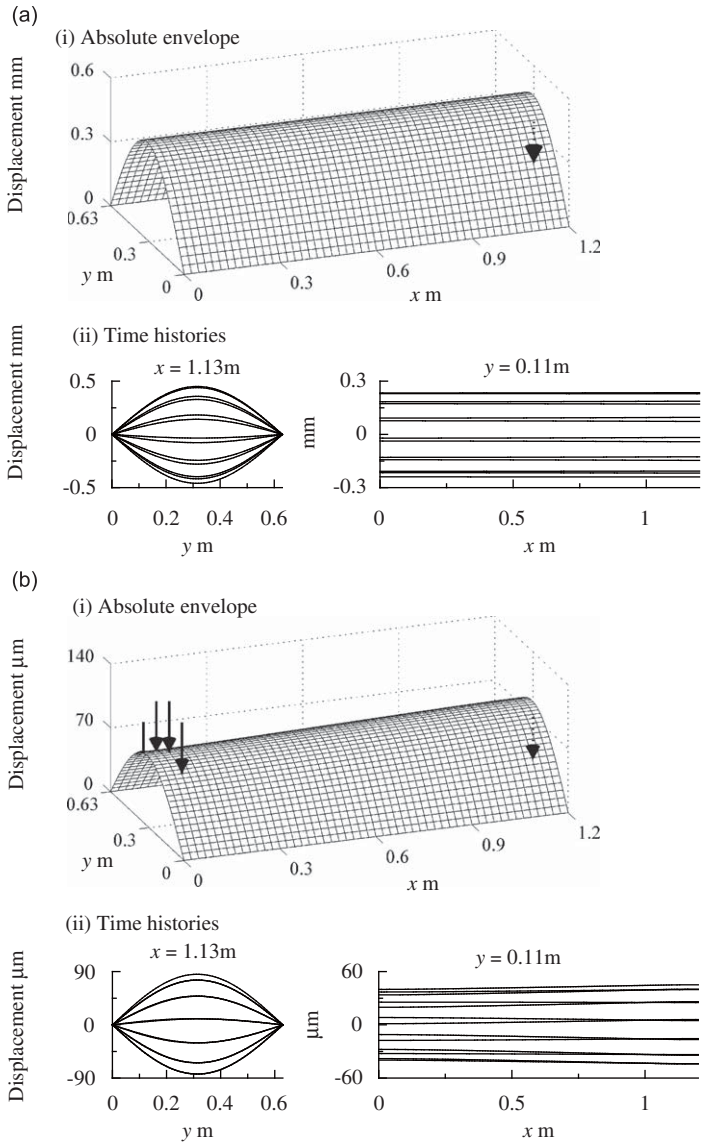

Fig. 9. Envelopes of absolute displacement of the panel at the first modal frequency with and without the RWAC and the corresponding time histories along the lines at $x = 1.13$ m and $y = 0.11$ m when the boundary conditions at the both ends of the panel is the sliding supports; the dotted arrow is a disturbance force and the solid arrows are control forces. (a) Without control (frequency: 24.38 Hz, $f_d = 0.5$ N): (i) absolute envelope; (ii) time histories. (b) With control (frequency: 24.38 Hz, $f_d = 0.5$ N): (i) absolute envelope; (ii) time histories.

disturbance forces is also the same as the previous cases. However, unlike in the case of Section 4.1, the control forces array is not fixed in the x direction through this section.

Case 4: *Pinned support*. In this part, the case is considered where the boundaries at $x = 0$ and $x = L_x$ are pinned-supported. Fig. 11 illustrates the gain plots of the dynamic compliances of the panel at the disturbance point and $(x, y) = (0.11\,\text{m}, 0.11\,\text{m})$ with and without the TWEC when the control forces array is set along $x_c = 0.86$ m. As is clear from Fig. 11(a), when the TWEC is applied, the extreme control effect which is more than suppressing resonance peaks is achieved in the controlled region. Although two peaks appear in this case, these result from the near-field in the controlled region which is affected by the newly produced mode in the uncontrolled region as shown in Fig. 11(b), thereby not indicating the modal excitation in the controlled region.

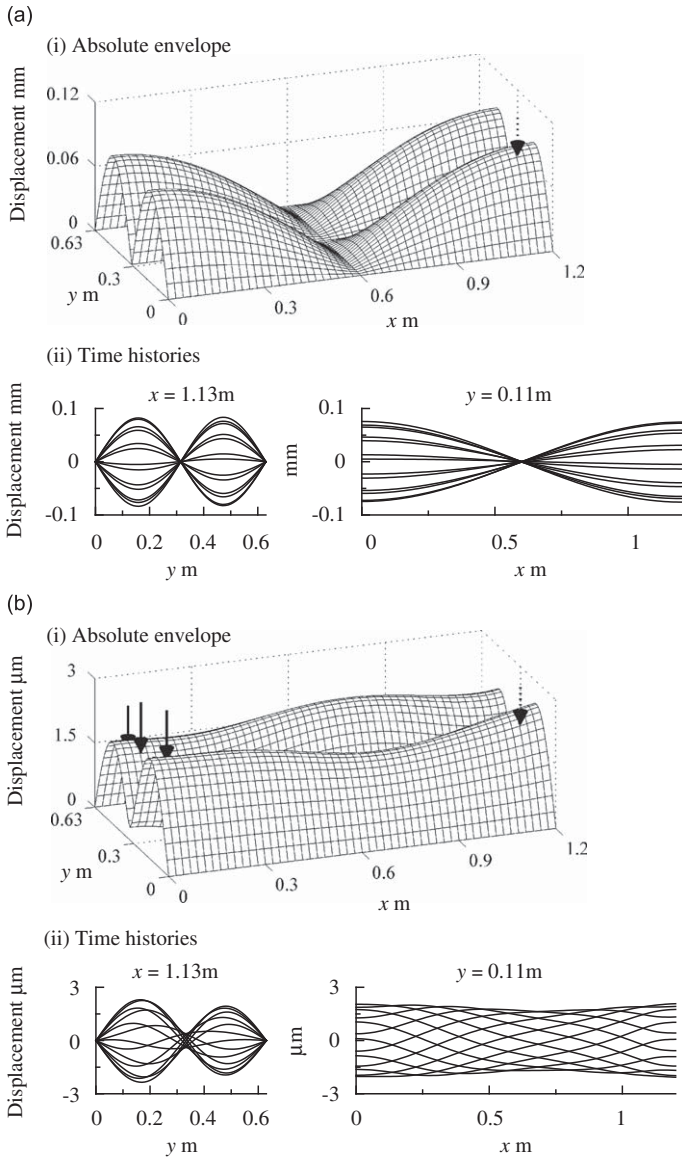

Fig. 10. Envelopes of absolute displacement of the panel at the sixth modal frequency with and without the RWAC and the corresponding time histories along the lines at $x = 1.13$ m and $y = 0.11$ m when the boundary conditions at the both ends of the panel are the sliding supports; the dotted arrow is a disturbance force and the solid arrows are control forces. (a) Without control (frequency: 104.25 Hz, $f_d = 0.5$ N): (i) absolute envelope; (ii) time histories. (b) With control (frequency: 104.25 Hz, $f_d = 0.5$ N): (i) absolute envelope; (ii) time histories.

This result is also observed in the case of active wave control for a one-dimensional structure [10]. Furthermore, in Fig. 11(b), the level of the asymptote is more reduced as the frequency increases up to approximately 200 Hz since the displacement in the controlled region mainly depends on the near-fields, that is, real exponential functions. Then, the gain curve rapidly increases after approximately 250 Hz. This is because the influence of the higher order modes that are not targeted in the control system becomes strong.

Next, the control effect is evaluated from a viewpoint of displacement distribution. Fig. 12 shows the envelopes of absolute displacement of the panel at the fourth modal frequency with and without the TWEC and the corresponding time histories. It should be noted that the displacement in the controlled region is

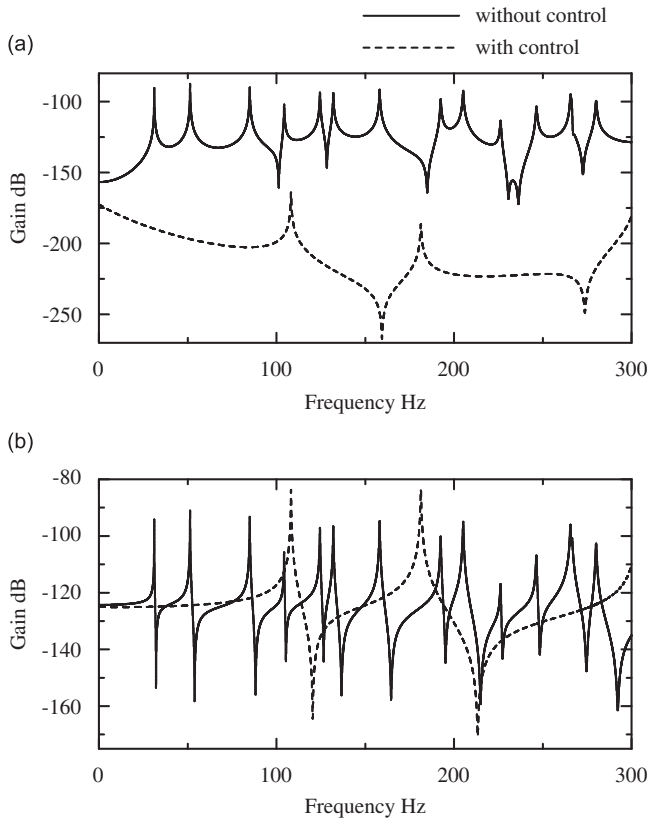

Fig. 11. Gain plots of the dynamic compliances of the panel at the disturbance point and $(x, y) = (0.11\,\text{m}, 0.11\,\text{m})$ with and without the TWEC when the control forces array is set along $x_c = 0.86\,\text{m}$ and the boundary conditions at the both ends of the panel are the pinned supports.

significantly suppressed, an almost vibration-free state being produced. This unique control effect implies that near-field components are dominant in the controlled region. Especially, the near-fields and progressive waves cannot couple at the pinned support boundary [24], and hence the transmitted wave cancellation results in nullifying the reflected waves in the controlled region (although the reference is concerned with a flexible beam, the characteristics of the boundary conditions is analogous to that of a rectangular panel since the one-dimensional waves are treated in this paper).

Case 5: *Free end*. In this part, the case is considered where the boundary conditions at $x = 0$ and $x = L_x$ are free. Depicted in Fig. 13 is the gain plots of the dynamic compliances of the panel at the disturbance point and $(x, y) = (0.11\,\text{m}, 0.11\,\text{m})$ with and without the TWEC when the control forces array is set along $x_c = 0.86\,\text{m}$. As is apparent from the figure, although the asymptote of the gain curve is extremely suppressed, the number of peaks with the TWEC is more than the Case 4. The characteristics of these peaks are divided into two categories; one results from newly produced modes in the uncontrolled region as with the Case 4 and the other from boundary condition in the controlled region as with the Case 2. In order to make the difference clearer, Fig. 14 shows the gain plots of the dynamic compliances at $(x, y) = (0.11\,\text{m}, 0.11\,\text{m})$ with the TWEC versus the position of the control forces array in the x direction. The shift of peak frequencies indicates the influences of the vibration modes in the uncontrolled region since the resonance frequencies are determined by the area of the uncontrolled region. Thus, the peak frequencies become higher as the control forces array shifts closer to the disturbance position. In contrast, the peaks that stay at the same frequencies after the position of the control forces array is changed indicate the influence of the free end along $x = 0$. If this is the case, the resonance in the x direction does not appear in the controlled region, and thus the structure behaves as a one-dimensional structure in the y direction as with the Case 2. Hence, the frequencies of the unmoved peaks are

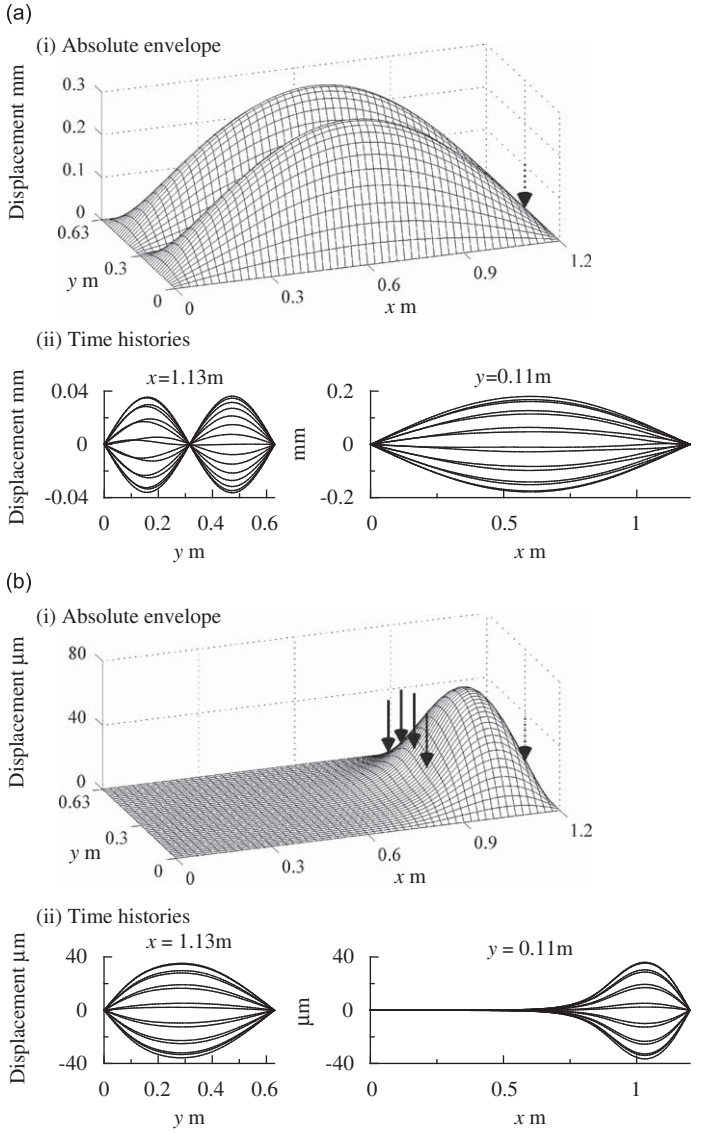

Fig. 12. Envelopes of absolute displacement of the panel at the fourth modal frequency with and without the TWEC and the corresponding time histories along the lines at $x = 1.13$ m and $y = 0.11$ m when the boundary conditions at the both ends of the panel are the pinned supports; the dotted arrow is a disturbance force and the solid arrows are control forces. (a) Without control (frequency: 104.22 Hz, $f_d = 10$ N): (i) absolute envelope; (ii) time histories. (b) With control (frequency: 104.22 Hz, $f_d = 10$ N): (i) absolute envelope; (ii) time histories.

coincident with those of the pinned-supported beam which has the same length in the y direction and physical parameters as the panel.

Then, consider the displacement distribution of the panel when the control forces array is placed at $x = 0.86$ m. Fig. 15 depicts the envelopes of absolute displacement of the panel and the corresponding time histories with and without the TWEC at 23.34 Hz where the unmoved peak exists as shown in Fig. 14. Although the maximum amplitude in the controlled region is smaller than that in the uncontrolled region, an almost vibration-free state is not generated unlike in the Case 4. As discussed in the Case 2, the controlled region where a progressive wave is nullified is sensitive (see Fig. 6) since the panel behaves as the pinned-supported beam which has the resonance at this frequency. Furthermore, the near-field decaying from the

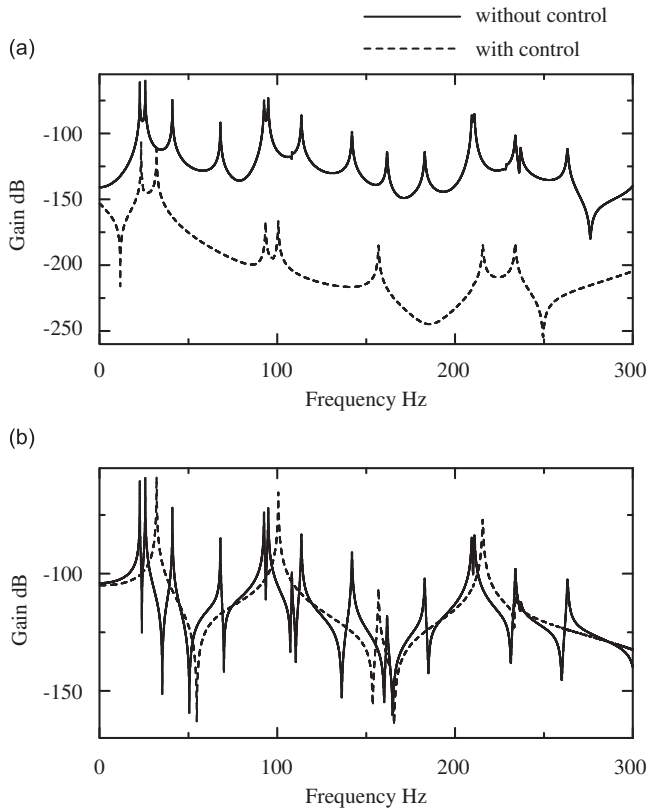

Fig. 13. Gain plots of the dynamic compliances of the panel at the disturbance point and $(x, y) = (0.11\,\text{m}, 0.11\,\text{m})$ with and without the TWEC when the control forces array is set along $x_c = 0.86\,\text{m}$ and the boundary conditions at the both ends of the panel are free.

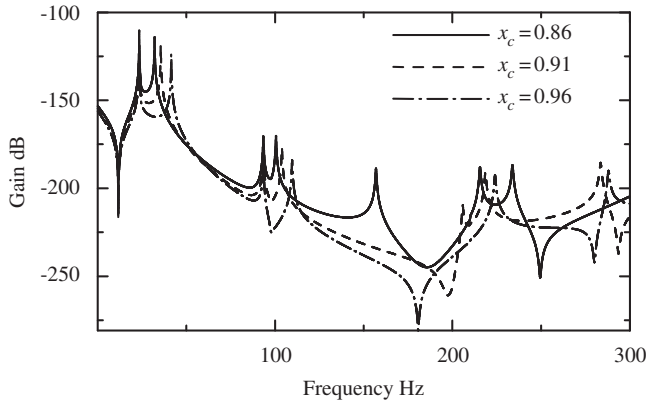

Fig. 14. Gain plots of the dynamic compliances at $(x, y) = (0.11\,\text{m}, 0.11\,\text{m})$ with the TWEC versus the position of the control forces array in the x direction when the boundary conditions at the both ends of the panel are free.

control forces array to the negative direction has relatively large contribution at the left end because of its low frequency, so that the large wave reflection occur at the free end, relatively large displacement remaining after control in the controlled region. Illustrated in Fig. 16 is the envelope of absolute displacement with the TWEC at 32.02 Hz where a resonance phenomenon appears in the uncontrolled region. In contrast to Fig. 15, the

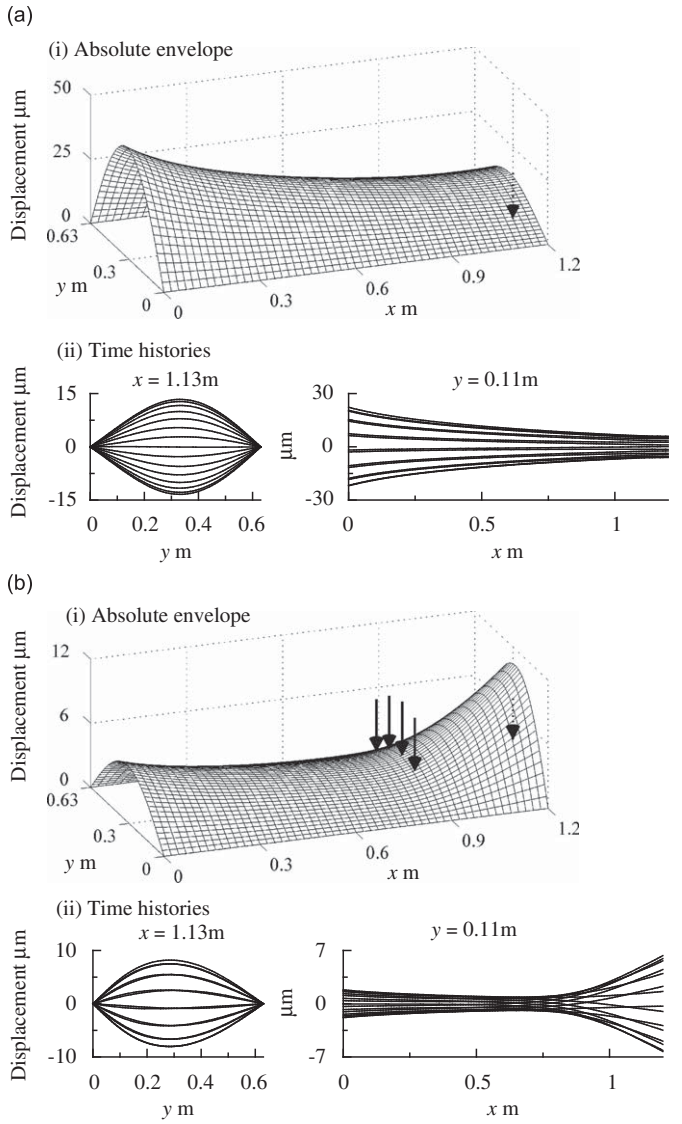

Fig. 15. Envelopes of absolute displacement of the panel at 23.34 Hz with and without the TWEC and the corresponding time histories along the lines at $x = 1.13$ m and $y = 0.11$ m when the boundary conditions at the both ends of the panel are free; the dotted arrow is a disturbance force and the solid arrows are control forces. (a) Without control (frequency: 23.34 Hz, $f_d = 0.5$ N): (i) absolute envelope; (ii) time histories. (b) With control (frequency: 23.34 Hz, $f_d = 0.5$ N): (i) absolute envelope; (ii) time histories.

displacement in the controlled region is smaller than that in the uncontrolled region. Although the shape of the displacement distribution is similar to the Case 4, this is not an almost vibration-free state since the newly produced mode affects the displacement in the controlled region with the near-field. However, in the region which is distant from the control forces array, the displacement is not so changed compared to the case of non-control.

Fig. 17 shows the envelopes of absolute displacement and the corresponding time histories with the TWEC at the fourth modal frequency. As is apparent from the figure, an almost vibration-free state is realized in this case since the amplitude in the controlled region is extremely reduced compared to the case of non-control. This is because the uncontrolled region and free end at $x = 0$ are off resonance at the frequency unlike the previous examples.

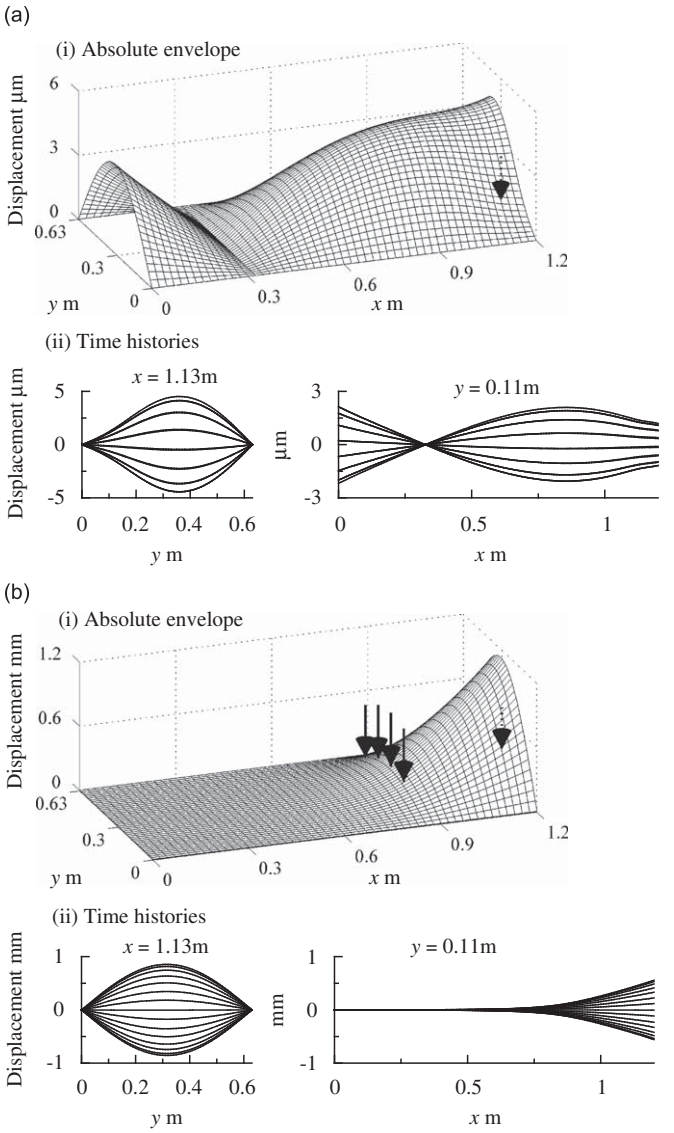

Fig. 16. Envelopes of absolute displacement of the panel at 32.02 Hz with and without the TWEC and the corresponding time histories along the lines at $x = 1.13$ m and $y = 0.11$ m when the boundary conditions at the both ends of the panel are free; the dotted arrow is a disturbance force and the solid arrows are control forces. (a) Without control (frequency: 32.02 Hz, $f_d = 0.5$ N): (i) absolute envelope; (ii) time histories. (b) With control (frequency: 32.02 Hz, $f_d = 0.5$ N): (i) absolute envelope; (ii) time histories.

Case 6: *Sliding support*. In this part, the case is considered where the boundary conditions at $x = 0$ and $x = L_x$ are sliding supports. Illustrated in Fig. 18 are the gain plots of the dynamic compliances of the panel at the disturbance point and $(x, y) = (0.11\text{ m}, 0.11\text{ m})$ with and without the TWEC when the control forces array is set along $x_c = 0.86$ m. As is clear from the figure, the asymptote is extremely suppressed in the controlled region. Although there exists five resonance peaks in the gain plot, those result from the vibration modes newly produced in the uncontrolled region as with the previous cases. Furthermore, the slope at $x = 0$ is constrained by the sliding support, so that the edge at $x = 0$ cannot behave as a pinned-supported beam unlike in Cases 2 and 5. It should be noted that resonance peaks do not exist at the frequencies of the lowest order vibration modes at each index, n, unlike in the case of the RWAC (see Fig. 8). As previously described, the controlled component in the active wave control system is not a progressive wave at these frequencies, and

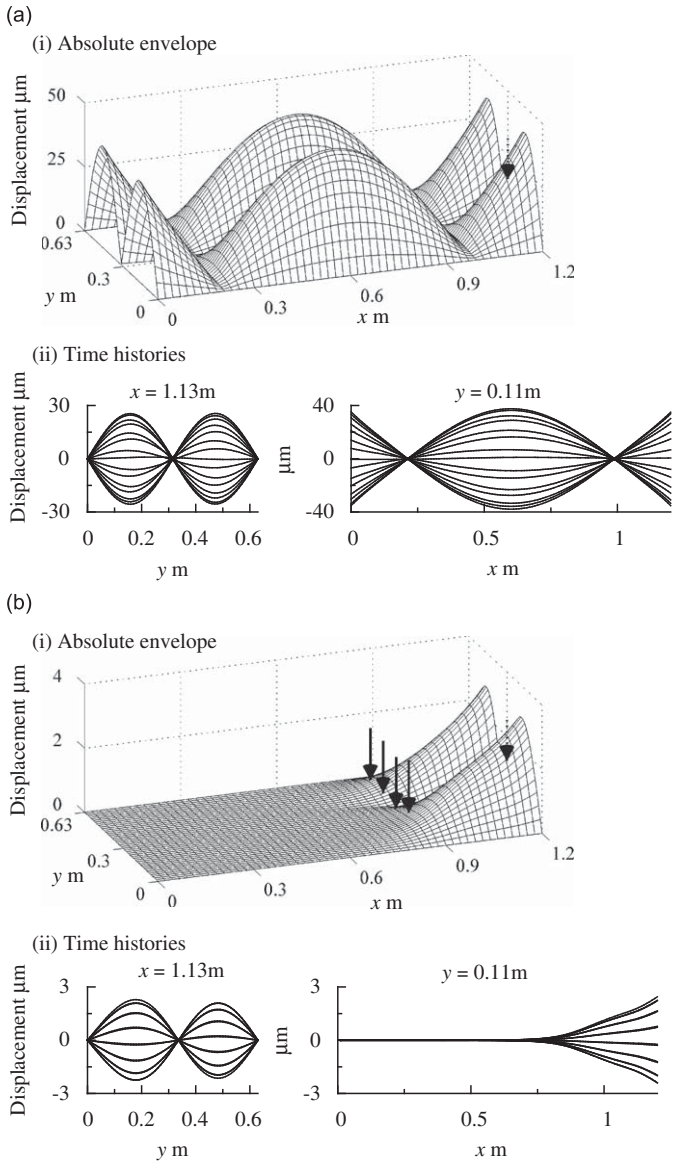

Fig. 17. Envelopes of absolute displacement of the panel at the fourth modal frequency with and without the TWEC and the corresponding time histories along the lines at $x = 1.13$ m and $y = 0.11$ m when the boundary conditions at the both ends of the panel are free; the dotted arrow is a disturbance force and the solid arrows are control forces. (a) Without control (frequency: 113.49 Hz, $f_d = 0.5$ N): (i) absolute envelope; (ii) time histories. (b) With control (frequency: 113.49 Hz, $f_d = 0.5$ N): (i) absolute envelope; (ii) time histories.

hence the RWAC cannot inactivate the vibration modes. If this is the case, the resonance phenomena are caused by the standing wave in the y direction. However, in the case of the TWEC, it aims to nullify the wave transmission at the control forces array, which indicates the suppression of the energy input into the controlled region. It is evident from the displacement distribution without the TWEC shown in Fig. 9 (or see Fig. 19) that the constant component to be controlled has much contribution to the displacement in the controlled region. Therefore, the suppression of such a component does not lead to the result that the resonance peaks at the frequencies remain.

Next, the control effect is evaluated from a viewpoint of displacement distribution. Fig. 19 shows the envelopes of absolute displacement of the panel at the first modal frequency with and without the TWEC and

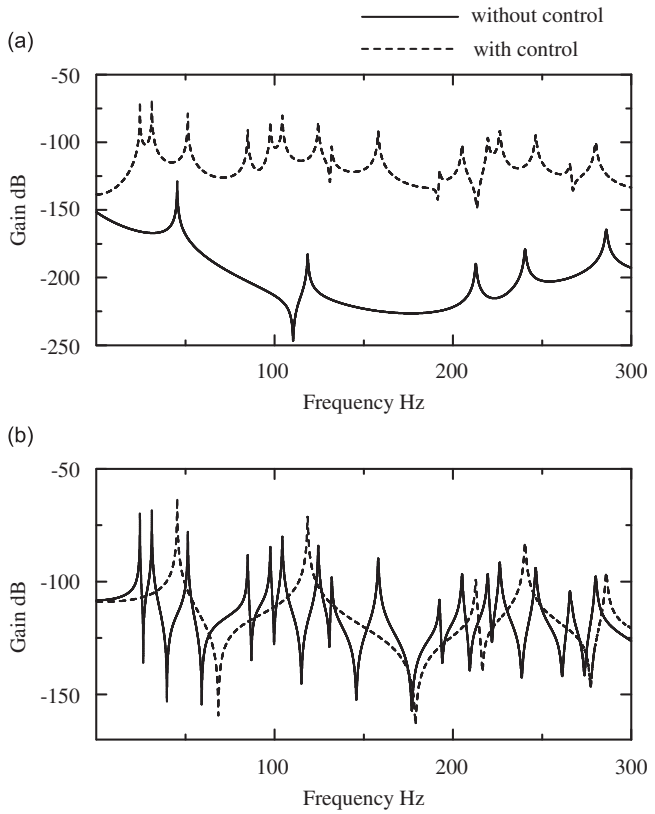

Fig. 18. Gain plots of the dynamic compliances of the panel at the disturbance point and $(x, y) = (0.11\,\text{m}, 0.11\,\text{m})$ with and without the TWEC when the control forces array is set along $x_c = 0.86\,\text{m}$ and the boundary conditions at the both ends of the panel are the sliding supports.

the corresponding time histories. As is clear from the figure, an almost vibration-free state is generated in this case since the amplitude in the controlled region is significantly suppressed. It should be noted that the contribution of the near-field in the controlled region is small while the excitation frequency is relatively low. Thus, when the boundary conditions at the both ends of the panel are the sliding supports, the TWEC is able to generate an almost vibration-free state at the lowest resonance frequency.

5. Conclusion

This paper has proposed active wave control of a finite rectangular panel, clarifying the validity of the control system. First, using a transfer matrix method of a rectangular panel, two kinds of active wave control laws were derived; the reflected wave absorbing control (RWAC) and the transmitted wave eliminating control (TWEC). Each control scheme is including the modal actuation in the direction orthogonal to the target wave. Control effects of the proposed method are then evaluated from a viewpoint of frequency response and displacement distribution. In general, the RWAC enables the inactivation of vibration modes and the TWEC enables an almost vibration free state. However, under some cases of boundary conditions, the proposed method has some properties different from the active wave control for a one-dimensional structure as follows:

(1) When the boundary condition parallel to the y-axis in the control region is free, new resonance phenomena appear in the direction orthogonal to the target wave after active wave control is applied.

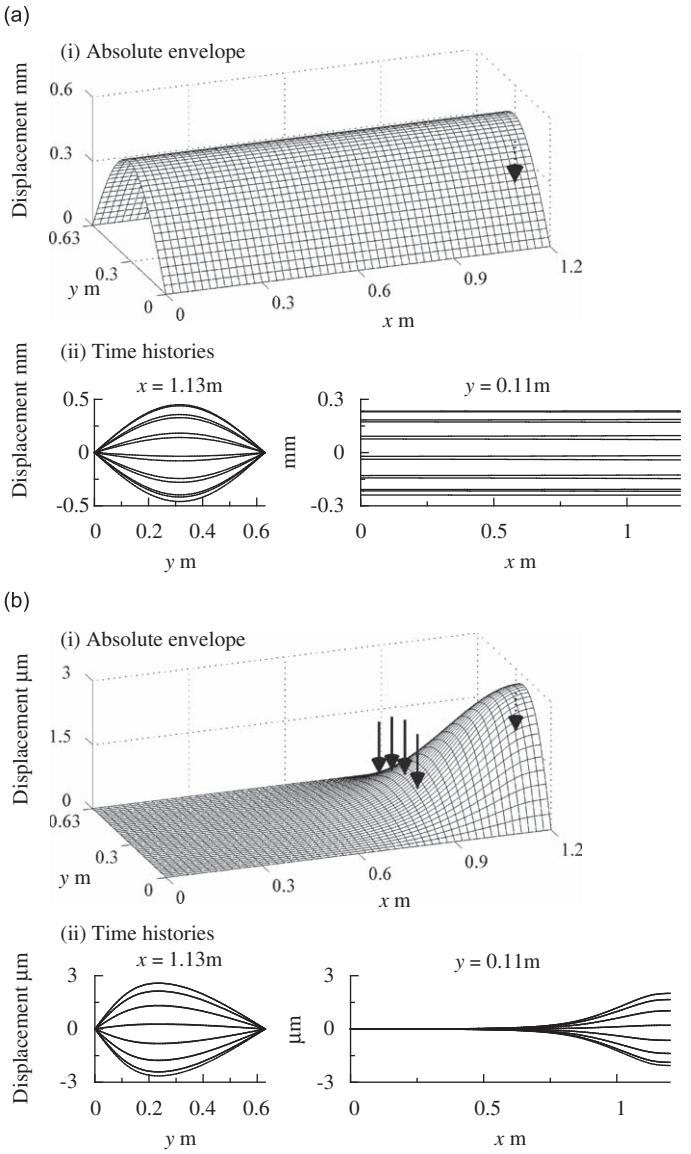

Fig. 19. Envelopes of absolute displacement of the panel at the first modal frequency with and without the TWEC and the corresponding time histories along the lines at $x = 1.13$ m and $y = 0.11$ m when the boundary conditions at the both ends of the panel are the sliding supports; the dotted arrow is a disturbance force and the solid arrows are control forces. (a) Without control (frequency: 24.38 Hz, $f_d = 0.5$ N): (i) absolute envelope; (ii) time histories. (b) With control (frequency: 24.38 Hz, $f_d = 0.5$ N): (i) absolute envelope; (ii) time histories.

(2) If the boundary conditions at the both ends of the panel are sliding supports, the RWAC cannot sufficiently suppress the lowest order modes for each modal index, n. This is because the target wave component is not a progressive wave but a constant at the frequencies.

In the case of active wave control for a beam-like structure, its control effects are the same for any boundary condition. However, as described above, the control effects of active wave control for a finite rectangular panel are dominated by the boundary conditions. Therefore, in order to achieve the same control effect as the active wave control for a one-dimensional structure, the displacement at the end boundary in the controlled region should be constrained.

Acknowledgement

Financial support for this work from the Japan Society for the Promotion of Science (Project no. 18860062) is gratefully acknowledged.

References

[1] L.A. Gould, M.A. Murray-Lasso, On the modal control of distributed systems with distributed feedback, *IEEE Transactions on Automatic Control* AC-11 (1966) 729–737.
[2] L. Meirovitch, H. Baruh, Implementation of modal filters for control of structures, *Journal of Guidance, Control, and Dynamics* 8 (1985) 707–716.
[3] D.R. Morgan, An adaptive modal-based active control system, *Journal of the Acoustical Society of America* 89 (1991) 248–256.
[4] R.A. Canfield, L. Meirovitch, Integrated structural design and vibration suppression using independent modal space control, *AIAA Journal* 32 (1994) 2053–2060.
[5] N. Tanaka, Y. Kikushima, Active modal control and its robustness using point sensors and point actuators, *JSME International Journal Series C* 42 (1999) 54–61.
[6] D.R. Vaughan, Application of distributed parameter concepts to dynamic analysis and control of bending vibration, *Journal of Basic Engineering* (1968) 157–166.
[7] A.H. von Flotow, J.B. Schafer, Wave absorbing controllers for a flexible beam, *Journal of Guidance, Control, and Dynamics* 9 (1986) 673–680.
[8] B.R. Mace, Active control of flexural vibrations, *Journal of Sound and Vibration* 114 (1987) 253–270.
[9] B.J. Brevart, C.R. Fuller, Active control of coupled wave propagation in fluid-filled elastic cylindrical shells, *Journal of the Acoustical Society of America* 94 (1993) 1467–1475.
[10] J.L. Svensson, P.B.U. Andersson, J. Scheuren, W. Kropp, Active scattering control of flexural waves at beam junctions: the influence of beam properties on power flow and control effect, *Journal of Sound and Vibration* 313 (2008) 418–432.
[11] N. Tanaka, Y. Kikushima, Active wave control of a flexible beam (proposition of the active sink method), *JSME International Journal Series C* 34 (1991) 159–167.
[12] N. Tanaka, Y. Kikushima, Active wave control of a flexible beam (fundamental characteristics of an active sink system and its verification), *JSME International Journal Series C* 35 (1992) 236–244.
[13] N. Tanaka, Y. Kikushima, Active wave control of a flexible beam (on the power flow control), *Transactions of the Japan Society of Mechanical Engineers C* 58 (1992) 2578–2585.
[14] S.J. Elliott, L. Billet, Adaptive control of flexural waves propagating in a beam, *Journal of Sound and Vibration* 163 (1993) 295–310.
[15] G.P. Gibbs, C.R. Fuller, R.J. Silcox, Active control of flexural and extensional power flow in beams using real time wave vector sensors, *Proceedings of the Second Conference on Recent Advances in Active Control of Sound and Vibration*, Blacksburgh, VA, 1993, pp. 909–925.
[16] H. Iwamoto, N. Tanaka, Active wave control of a flexible beam using wave filter constructed with four point sensors, *Proceedings of Asia-Pacific Vibration Conference 2003*, Gold Coast, November 2003, pp. 210–215.
[17] H. Iwamoto, N. Tanaka, Adaptive feedforward control of flexural waves propagating in a beam using smart sensors, *Smart Materials and Structures* 14 (2005) 1369–1376.
[18] C.R. Halkyard, B.R. Mace, Adaptive active control of flexural waves in a beam in the presence of a nearfield, *Journal of Sound and Vibration* 285 (2005) 149–171.
[19] X. Pan, C.H. Hansen, Active control of vibratory power transmission along a semi-infinite plate, *Journal of Sound and Vibration* 184 (1995) 585–610.
[20] A.J. Young, C.H. Hansen, Control of flexural vibration in a stiffened plate using piezoceramic actuators and an angle stiffener, *International Journal of Active Control* 1 (1995) 277–301.
[21] N.J. Kessissoglou, Active control of the plate energy transmission in a semi-infinite ribbed plate, *Journal of the Acoustical Society of America* 107 (2000) 324–331.
[22] N.J. Kessissoglou, An analytical and experimental investigation on active control of the flexural wave transmission in a simply supported ribbed plate, *Journal of Sound and Vibration* 240 (2001) 73–85.
[23] A. Sakano, N. Tanaka, Active progressive wave control of a simply supported plate, *JSME International Journal Series C* 46 (2003) 867–872.
[24] B.R. Mace, Wave reflection and transmission in beams, *Journal of Sound and Vibration* 97 (1984) 237–246.